Journal of Power Sources 262 (2014) 232–238

Contents lists available at ScienceDirect

Journal of Power Sources

journal homepage: www.elsevier.com/locate/jpowsour

Multi-laminated copper nanoparticles deposited on conductive substrates for electrocatalytic oxidation of methanol in alkaline electrolytes

Lun-Peng Xia [a], Peng Guo [a], Yan Wang [a], Shi-Qi Ding [b], Jian-Bo He [a,*]

[a] Anhui Key Lab of Controllable Chemical Reaction & Material Chemical Engineering, School of Chemical Engineering, Hefei University of Technology, Hefei 230009, China
[b] Anhui Tongguan Copper Foil Company, Chizhou 247000, China

HIGHLIGHTS

- A simple electrodeposition approach to grow multi-laminated copper particles.
- Cu particles with preferentially oriented {111} planes parallel to the substrate.
- Solid carbon paste coated with PAMT film as a support of Cu catalyst.
- Excellent catalytic activity to methanol oxidation in alkaline electrolytes.
- PAMT interlayer facilitating electron transfer kinetics of methanol oxidation.

GRAPHICAL ABSTRACT

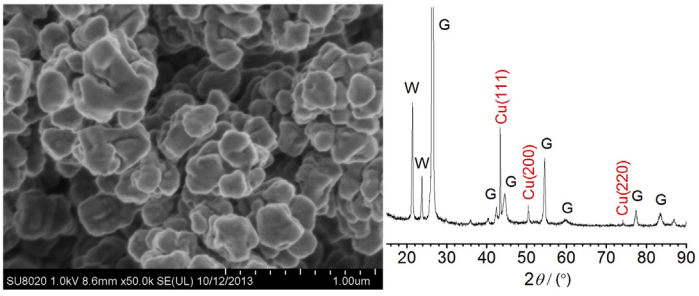

ARTICLE INFO

Article history:
Received 26 February 2014
Received in revised form
27 March 2014
Accepted 28 March 2014
Available online 4 April 2014

Keywords:
Multi-laminated particles
Solid carbon paste electrode
Conducting polymer
2-Amino-5-mercapto-1,3,4-thiadiazole
Electrocatalysis
Direct methanol fuel cell

ABSTRACT

A simple electrodeposition approach to grow multi-laminated copper particles on two conductive substrates is presented. Morphological and structural characterization was performed using SEM and XRD. The copper crystallites are preferentially oriented with {111} planes parallel to the substrate surfaces, providing an optimum interface for methanol oxidation. There are a large number of edges, corners, and atomic steps around individual multi-laminated nanostructured particles. The excellent electrocatalytic activity of the particles to methanol oxidation in alkaline solutions is demonstrated by cyclic voltammetry, electrochemical impedance spectroscopy and chronoamperometry. The presence of the conductive poly(2-amino-5-mercapto-1,3,4-thiadiazole) interlayer between the Cu particles and the carbon paste substrate results in larger specific surface areas of the particles and smaller charge-transfer resistances of methanol oxidation reaction in the lower potential range. Such an anisotropic laminated structure of non-noble metal nanomaterials deserves further investigation for finding a suitable alternative to noble metal-based anodic catalysts in fuel cells.

1. Introduction

The direct methanol fuel cell (DMFC) is one of the most promising power sources for electronic portable devices, because of its low working temperature, high energy conversion efficiency,

* Corresponding author. Tel.: +86 551 62904653; fax: +86 551 62901450.
E-mail address: jbhe@hfut.edu.cn (J.-B. He).

http://dx.doi.org/10.1016/j.jpowsour.2014.03.139
0378-7753/

low polluting emission, and convenient fuel storage and supply [1]. One of the main challenges of the DMFC system is the poor anodic reaction kinetics that causes large overpotentials and then relatively low power density. There are many studies in the area of the anodic catalysts of DMFCs, mainly focusing on noble metals [2,3] and their alloys such as PtRu [4,5], PtCu [6], Pt@AuCu [7], PdRu [8], and PdCu [9], and their other nanocomposites such as Pt/C [10], Pt–CuO/C [11], Pt/MoO_3/C [12], Pt/WO_3 [13], PdAg/TiO_2 [14], Pt–$LaFeO_3$–CNT–chitosan [15], and graphene–cobaltite–Pd [16]. Many novel catalyst supports are also developed, e.g. functionalized carbon-series nanomaterials [4,5,8] and conducting polymer films [2,3]. The main objects of developing nanocomposite catalysts and supports are to minimize the loadings of noble metals as well as to promote the methanol oxidation kinetics by facilitating the oxidation of the adsorbed CO reaction intermediate to CO_2.

Due to the high prices of noble metals, it is a useful direction to try and develop high performance non-noble metal anodic catalysts used in alkaline electrolytes. The development of anion-exchange membranes has provided the possibility of commercial applications of alkaline DMFCs. The most widely studied non-noble metals are Ni [17–25], Cu [26–31], and their alloys [32,33] and oxides [34]. These metallic nanoparticles were combined with nanocarbons [22,23,29,32], conducting polymers [17,20,21,23–25,30], and other inorganic [18,19,31,33] and organic [17,22,25] species, for the purpose of obtaining enhanced catalytic activity and long-term stability.

Copper nanostructures have recently received an increasing interest as the anodic catalyst of DMFCs in alkaline media. Copper electrodes were modified by electrocorrosion and electrodeposition, which enable to enhance the methanol oxidation reaction [27]. Anisotropic platelike copper microcrystals and nanocrystals, with enhanced catalytic activity for methanol oxidation, were synthesized on a gold-coated mica substrate in the presence of KBr as an additive [28]. Copper nanowire decorated reduced graphene oxide was synthesized by hydrothermal approach; the obtained composites exhibited a superior catalytic activity for methanol oxidation [29]. Copper-poly(2-aminodiphenylamine) composite was prepared as a novel and low cost electrocatalyst for methanol oxidation [30]. Copper-ceria hybrid electrode was also fabricated for electrocatalytic oxidation of methanol [31].

The geometry is a key factor in the development of nanomaterials for use as electrocatalysts. The geometry of the electrodeposited copper nanoparticles is strongly affected by the applied potential. Deposition at very high overpotentials, e.g. −4 V [7] or −6 V [35] vs Ag/AgCl/3 M KCl, can result in the formation of porous Cu foams assisted by strong hydrogen evolution. The copper particles grown at a very low overpotential of 0.06 V vs Ag/AgCl/3 M KCl tended to acquire anisotropic platelike morphology [28]. At a potential of −0.175 V vs Ag/AgCl/3 M KCl the obtained were the coarse grained closely packed copper clusters [30].

In the present work, Cu particles were electrodeposited on two very different substrates, a bare solid carbon paste electrode (sCPE) and a sCPE modified by an electropolymerized 2-amino-5-mercapto-1,3,4-thiadiazole (AMT) layer. The combination of sCPE with poly-AMT (PAMT) has been demonstrated in previous work in our group to be suitable as a support for the platinum electrocatalyst of a direct methanol fuel cell [3]. The originality of the present work lies in the fact that, by carefully selecting the deposition potential, multi-laminated Cu platelets with well-controlled orientation can be grown on both substrates, assisted by gentle hydrogen evolution. This nanostructure of Cu platelets has been proved in this study to possess highly catalytic activity to methanol oxidation in alkaline media.

2. Experimental

2.1. Chemicals and solutions

Spectrograde graphite powders (320 mesh) and spectrograde paraffin wax (solidification point 56–58 °C) were purchased from Sinopharm group for preparing the sCPE. AMT (98% + pure) was purchased from Alfa Aesar. Copper (II) sulfate pentahydrate, sodium hydroxide and all other chemicals were of analytical grade from Sinopharm Group. Doubly-distilled water from an all-glass distillatory apparatus was used as solvent.

The monomer solution for electropolymerization was 0.5 mmol dm^{-3} AMT in 0.1 mol dm^{-3} H_2SO_4. The solution for electrodeposition of copper contained 0.010 mol dm^{-3} $CuSO_4$ and 0.5 mol dm^{-3} H_2SO_4. The supporting electrolytes for methanol oxidation were 0.5 mol dm^{-3} NaOH containing CH_3OH at different concentrations.

2.2. Electrode preparation

A disk sCPE with a geometrical area of 0.1134 cm^2 was used as the substrate for fabricating the anode catalyst of DMFC. The preparation of sCPE was described previously [3]. The area of 0.1134 cm^2 was used for calculation of current density (j). The sCPE was polished with 800 grit abrasive paper followed by rinsing in double distilled water. Then the cleaned sCPE was activated by repetitive potential cycling between −0.4 and 1.6 V at 0.5 V s^{-1} in 1.0 mol dm^{-3} KCl until the background current became stable. On the surface of the activated sCPE, the polymerization of AMT monomer was performed by cyclic potential scan between −0.2 and 1.7 V vs SCE at 50 mV s^{-1} in the AMT solution. Thus, a PAMT-modified sCPE (PAMT/sCPE) was obtained. The cycle number for the electropolymerization was optimized in the range of 0–100 cycles according to the electrocatalytic activity towards methanol oxidation.

Copper particles were potentiostatically electrodeposited from the $CuSO_4$ solution onto the bare sCPE and PAMT/sCPE substrates, respectively. During the deposition course, a gentle evolution of hydrogen took place, which can affect the morphology of the deposited particles. The final Cu-loaded electrodes were denoted as Cu/sCPE and Cu/PAMT/sCPE.

2.3. Apparatus and procedures

Cyclic voltammetry (CV), electrochemical impedance spectroscopy (EIS) and chronoamperometry were performed on a CHI660C workstation (CH Instruments, Shanghai, China). The three-electrode system was composed of a Cu/PAMT/sCPE or a Cu/sCPE as working electrode, a KCl-saturated calomel reference electrode (SCE) and a platinum-coil counter electrode. All potentials in this work are referred to SCE. Before test, the working electrode was cleaned in double distilled water. All experiments were conducted at room temperature (approximately 25 °C).

Impedance spectra were recorded for methanol oxidation at different potentials. The EIS experiments were conducted in a frequency range from 0.1 Hz to 100 kHz with AC voltage amplitude of 5 mV. The obtained data was fitted to an appropriate equivalent circuit using the complex nonlinear least-squares method.

Surface morphologies of the two Cu-loaded electrodes were characterized using an SU8020 field-emission scanning electron microscope (FE-SEM, Hitachi, Japan). The structural properties of the deposited Cu were examined using a D/MAX2500V X-ray diffractometer (XRD, Rigaku, Japan) equipped with Ni filtered CuKα as the radiation source. The tube current was 40 mA with a voltage

of 40 kV. X-ray diffractograms were obtained for 2θ values ranging between 15° and 90°.

3. Results and discussion

3.1. Preparation and characterization of Cu-loaded electrodes

Electrooxidative polymerization of AMT monomer on sCPE was carried out by multi-cycle voltammetry under conditions chosen on the basis of our previous work [36]. The optimal deposition conditions for PAMT film are a combination of a solution of 0.5 mmol dm^{-3} AMT + 0.1 mol dm^{-3} H_2SO_4, a scan region between −0.2 V and 1.7 V vs SCE and a cycle number of 25. The electrodeposition of Cu was performed in a solution of 0.010 mol dm^{-3} $CuSO_4$ + 0.5 mol dm^{-3} H_2SO_4, and the applied potential and time were optimized as −0.80 V and 20 min, respectively. The deposition potential can influence the evolution rate of hydrogen and then affect the morphology of the deposited particles.

Fig. 1 shows the FE-SEM images of the prepared Cu/sCPE and Cu/PAMT/sCPE. Both samples exhibit an intricate three-dimensional geometry made from multi-laminated nanostructured platelets, with a top surface parallel to the substrates. The average size of the irregular platelets was *ca.* 0.3 × 0.3 μm^2 for Cu/sCPE and nearly half that for Cu/PAMT/sCPE. Individual platelet "bricks" seem to expand in horizontal direction but stop before they abut adjacent bricks, leaving lots of interstices between the particles and leading to a very large specific surface area. Also, a large number of edges, corners, and atomic steps were obtained and they are expected to be favorable for improving the catalytic activity. The platelet "bricks" on Cu/PAMT/sCPE had a smaller average size and therefore a larger specific surface area than on Cu/sCPE.

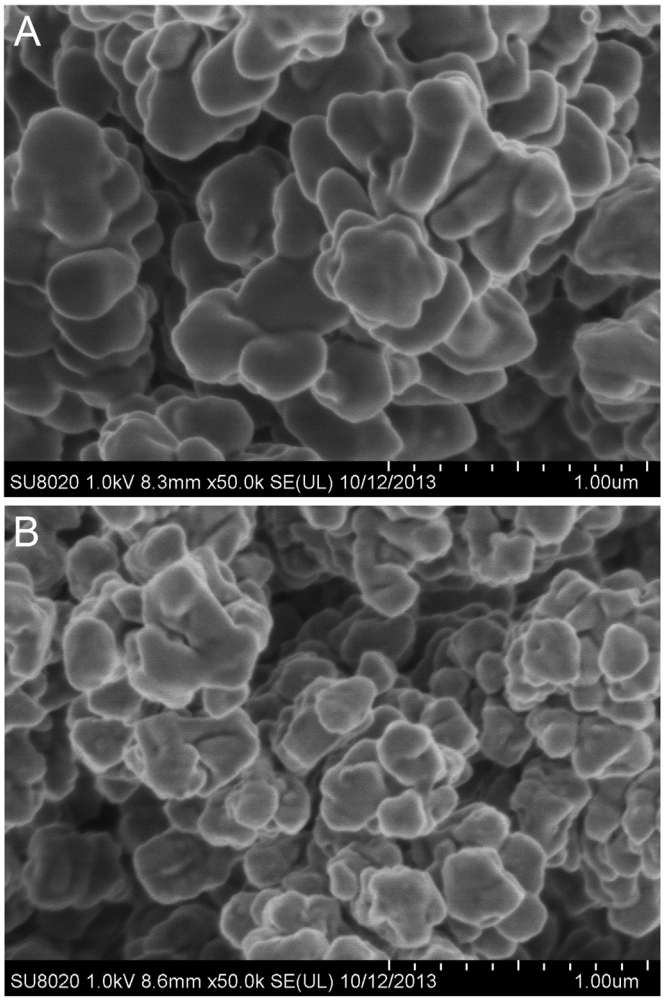

Fig. 1. FE-SEM images of Cu/sCPE (A) and Cu/PAMT/sCPE (B). The PAMT film was deposited on sCPE in 0.5 mmol dm^{-3} AMT + 0.1 mol dm^{-3} H_2SO_4 by CV scan between −0.2 V and 1.7 V vs SCE at 50 mV s^{-1} for 25 cycles. The Cu particles were deposited from 0.010 mol dm^{-3} $CuSO_4$ + 0.5 mol dm^{-3} H_2SO_4 at −0.80 V vs SCE for 20 min.

Fig. 2 shows XRD patterns of Cu/sCPE and Cu/PAMT/sCPE. Similar diffraction peaks were observed for both electrodes, independently from the presence of the PAMT interlayer. Besides the peaks assigned to graphite (G) and paraffin wax (W), one strong peak and two much weaker ones are present at 43.3°, 50.4° and 74°, which are indexed as the {111}, {200} and {220} crystal planes of face-centered cubic Cu (JCPDS No. 3-2838), respectively. The intensity ratios of the {200} to the {111} diffraction peaks were calculated to be 0.23 for Cu/sCPE and 0.18 for Cu/PAMT/sCPE, both of which are smaller than the bulk value of 0.47. Accordingly, the {111} planes are preferentially oriented parallel to the substrate surfaces. It was recently reported that the {111} and {110} crystal planes of copper had enhanced catalytic activity to methanol oxidation in comparison to the {100} crystal plane of copper [28]. As seen in Fig. 1, the anisotropic laminated structure allows the active {111} crystal plane exposed fully, which is favorable for the catalytic activity to methanol oxidation.

The apparent total thicknesses of the laminated Cu deposits were examined through galvanostatic stripping chronopotentiometry. A constant oxidation current of 1.0 mA was applied on Cu/sCPE and Cu/PAMT/sCPE in 1.0 mol dm^{-3} H_2SO_4. Two transient times of 95 and 110 s for anodic dissolution of Cu were

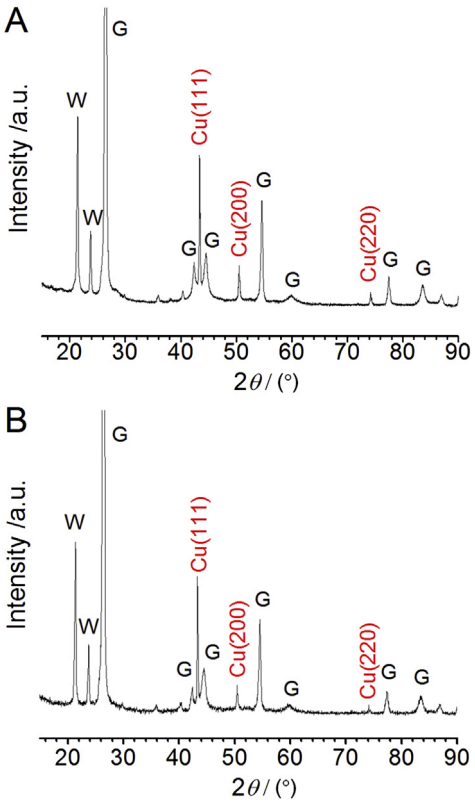

Fig. 2. XRD patterns of Cu/sCPE (A) and Cu/PAMT/sCPE (B). The electrodes were prepared under the same conditions as in Fig. 1.

obtained on the chronopotentiometric curves of Cu/sCPE and Cu/PAMT/sCPE (data not shown), respectively. The masses of the Cu deposits were calculated to be 275 and 319 μg cm^{-2}, corresponding to two thicknesses of 308 and 356 nm for the Cu layers on Cu/sCPE and Cu/PAMT/sCPE, respectively.

3.2. Electrocatalytic oxidation of methanol

The electrocatalytic effects of Cu/sCPE and Cu/PAMT/sCPE on methanol oxidation were evaluated by cyclic voltammetry in 0.5 mol dm^{-3} NaOH. Fig. 3A and B shows the CV curves of the first cycle, recorded at a scan rate (v) of 50 mV s^{-1} on the two electrodes. In the absence of methanol, four anodic peaks, I, II, II′, and III, occurred at −0.41, −0.16, 0.01, and 0.64 V (curves a), respectively, which are assigned to the formation of Cu(I), Cu(II), and Cu(III) species [26,37,38]. The reaction equations corresponding to various peaks can be found in literature [26]. An extraordinarily high current density was observed for peak II′ on both electrodes, especially on Cu/PAMT/sCPE. This peak is related to the formation of soluble Cu(II) species; the high peak currents can be attributed to the large specific surface area and quite a lot of active sites. Moreover, all four peak current densities at both electrodes are much larger than their respective values obtained with a polished copper electrode (curve c in Fig. 3B). For example, the peak current densities of peak I at Cu/sCPE and Cu/PAMT/sCPE are 8 and 8.7 times, respectively, as high as that at the polished copper electrode.

In the presence of 0.5 mol dm^{-3} methanol (curves b in Fig. 3A and B), peak III was replaced by a remarkably high anodic peak resulting from oxidation of methanol. The onset potential of the electrocatalytic oxidation appeared at *ca.* 0.4 V vs SCE, which is lower than those at the electrochemical-treated Cu electrodes [27], platelike Cu particles [28], CuNW–GCE and CuNW@RGO-GCE [29], Cu/P(2ADPA)/MCPE [30], and Cu–CeO_2/Cu [31]. Moreover, the onset potentials for methanol oxidation on both electrodes are evidently lower than that of peak III (near to 0.6 V). The slight increase in current density before peak III is due to the slow, potential-driven formation of Cu(I) and Cu(II) oxides at the interface between Cu substrate and the oxide coatings, as discussed in Ref. [37]. Peak III is associated with the formation of Cu(III) species, which has been generally reported to be a redox mediator in the oxidation of methanol on Cu-loaded electrodes [26–31]. In our work, however, the catalytic oxidation of methanol has occurred before the scan reaches the potential required for Cu(III) formation. This result does not support the Cu(III)-mediated electron transfer mechanism.

The peak of methanol oxidation remained high during the subsequent scan cycles, whereas all oxidation peaks of Cu disappeared completely after three cycles (Fig. 4). The solid Cu oxides formed in the initial cycles hinder the further oxidation of Cu, yet it is these oxides that catalyze the oxidation of methanol [39]. The Cu/PAMT/sCPE presents a higher peak current density (196 mA cm^{-2}) and a lower peak potential (0.838 V) than the Cu/sCPE (compare curves b with a), reflecting a positive effect of the PAMT film on methanol oxidation. No catalytic effect on methanol oxidation was observed for both PAMT/sCPE and sCPE (curves c and d).

Table 1 lists some non-noble metal modified electrodes recently reported for electrocatalytic oxidation of methanol in alkaline media. In comparison with previous works, the Cu/PAMT/sCPE exhibits excellent electrocatalytic activity to methanol oxidation.

3.3. EIS characterization

EIS is an effective tool for studying the interface properties of surface-modified electrodes. Fig. 5 shows the Nyquist plots of the two electrodes in 0.5 mol dm^{-3} CH_3OH + 0.5 mol dm^{-3} NaOH. The applied bias potentials ranged from 0.3 to 0.9 V vs SCE. The impedance spectra recorded at 0.3 V exhibited a quarter circle portion (curves a in Fig. 5A and B), corresponding to a large charge-transfer resistance. The spectra became a well-defined capacitive depressed semicircle with increasing potential from 0.3 to 0.6 V (curves b–d). The size of the semicircle decreased with increasing potential. At the potentials of 0.7, 0.8 and 0.9 V (curves e–g), the spectra showed a typical Nyquist plot including a semicircle portion

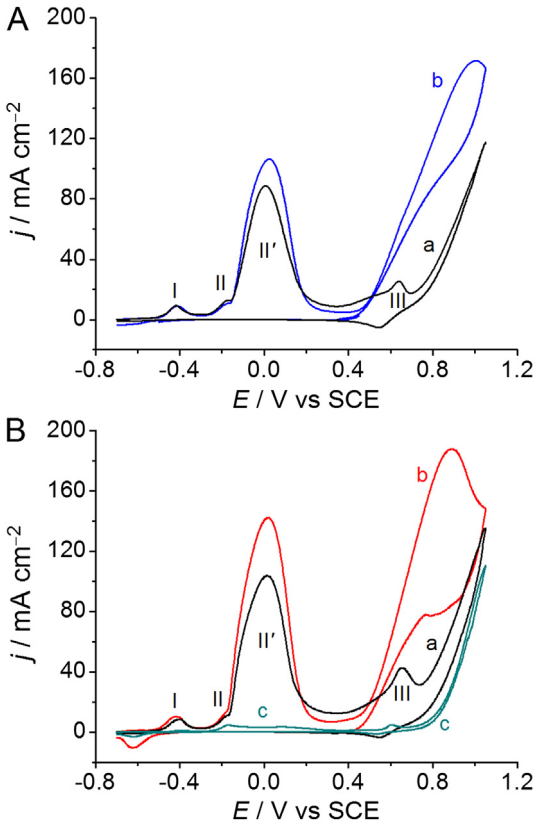

Fig. 3. CV curves of the first cycle on Cu/sCPE (A), Cu/PAMT/sCPE (B, a and b) and a polished Cu electrode (B, c) in 0.5 mol dm^{-3} NaOH in the absence (a and c) and presence (b) of 0.5 mol dm^{-3} methanol, v = 50 mV s^{-1}. The electrodes were prepared under the same conditions as in Fig. 1.

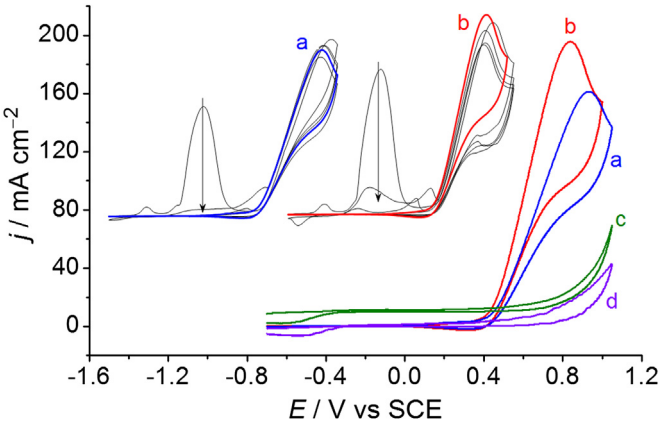

Fig. 4. CV curves on Cu/sCPE (a), Cu/PAMT/sCPE (b), PAMT/sCPE (c) and sCPE (d) in 0.5 mol dm^{-3} NaOH + 0.5 mol dm^{-3} methanol, v = 50 mV s^{-1}. The curves a and b illustrate the last cycle of the 5-cycle CV curves (the insets). The current densities of curves c and d have been magnified by 50 times for clearer view. The electrodes were prepared under the same conditions as in Fig. 1.

Table 1
Nanostructured non-noble metal composite electrodes recently reported for electrocatalytic oxidation of methanol in alkaline media. All the peak current densities (j_p) quoted in this table are referred to the electrode geometric areas available in the respective literature. All the peak potentials (E_p) have been converted to the values vs SCE for direct comparison.

Electrodes	CV parameters in CH_3OH oxidation				Ref.
	c/(mol dm^{-3})	v/(mV s^{-1})	E_p/V vs SCE	j_p/(mA cm^{-2})	
Ni/CTAB–PMT/MCPE	CH_3OH: 0.19 NaOH: 0.1	20	0.8	40	[17]
Ni/SBA/CPE	CH_3OH: 0.25 NaOH: 0.1	25	0.79	24	[18]
Ni–NiY/CPE	CH_3OH: 0.5 NaOH: 0.1	20	0.8	13.2	[19]
Ni/P-1,5-DAN/MCPE	CH_3OH: 0.57 NaOH: 0.1	10	0.64	1.5	[20]
Ni/PANI/CPE	CH_3OH: 0.5 NaOH: 0.1	25	0.55	16.7	[21]
Ni(II)–Qu–MWCNT-PE	CH_3OH: 0.4 NaOH: 0.1	20	0.7	18.5	[22]
Ni/POT(TX-100)/MWCNT-PE	CH_3OH: 0.24 NaOH: 0.1	20	0.67	18.5	[23]
Ni/POAP/MCPE	CH_3OH: 0.45 NaOH: 0.1	50	0.6	1.8	[24]
Ni/SDS–POAP	CH_3OH: 0.76 NaOH: 0.1	20	0.72	17.1	[25]
Platelike Cu particles	CH_3OH: 0.25 NaOH: 0.1	10	0.90	8.3	[28]
CuNW@RGO–GCE	CH_3OH: 1.0 NaOH: 0.1	50	0.84	109	[29]
Cu/P(2ADPA)/MCPE	CH_3OH: 0.5 NaOH: 0.2	10	0.82	46	[30]
Cu–CeO_2/Cu	CH_3OH: 0.4 NaOH: 0.1	10	0.86	7.8	[31]
CoCu/CNFs	CH_3OH: 2 KOH: 1	50	0.8	18	[32]
Ni–Cu–P/C	CH_3OH: 0.5 KOH: 0.1	10	0.69	9.5	[33]
$NiCo_2O_4$/GCE	CH_3OH: 1 NaOH: 0.1	50	0.64	15.5	[34]
Cu/PAMT/sCPE	CH_3OH: 0.5 NaOH: 0.5	50	0.838	196 at 0.838 V 148 at 0.7 V	This work

Abbreviation: CATB–PMT = cetyltrimethyl ammonium bromide–poly(*m*-toluidine); SBA = mesoporous silica; NiY = Ni(II) incorporated in zeolite Y; P-1,5-DAN = poly(1,5-diaminonaphthalene); MCPE = modified carbon paste electrode; PANI = polyaniline; Qu = quercetin; MWCNT-PE = multiwall carbon nanotube paste electrode; POT = poly(*o*-toluidine); TX-100 = triton X-100; POAP = poly(*o*-aminophenol); SDS = sodium dodecyl sulfate; CuNW = Cu nanowire; RGO = reduced grapheme oxide; P(2ADPA) = poly(2-aminodiphenylamine); CNFs = carbon nanofibers.

in higher frequency range and a linear portion in lower frequency range, corresponding to the electron transfer-limited and the diffusion-limited processes, respectively. No low-frequency inductive loop was observed for both electrodes at any potential, suggesting the absence of intermediate adsorbates. Inductive behavior has been explained by Müller et al. [40] using the kinetic theory derived by Harrington and Conway [41] for the reactions involving intermediate adsorbates. The intermediate adsorbates may cause self-poisoning of the electrode surface, as generally observed at a Pt-loaded electrode [3].

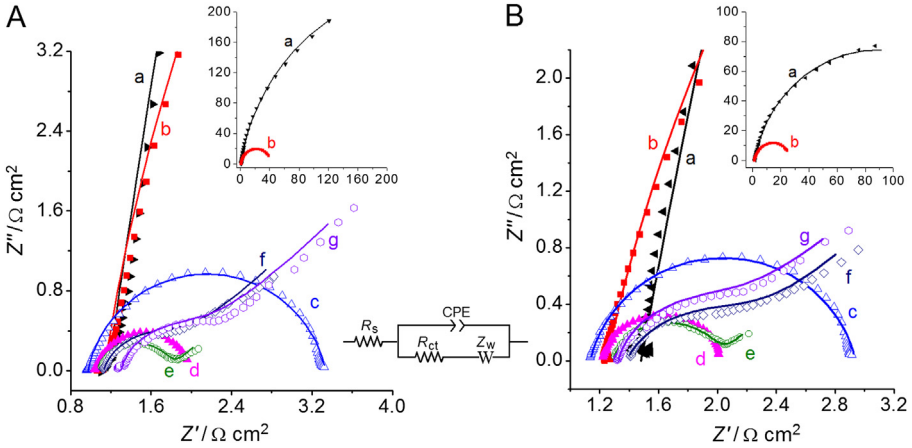

Fig. 5. Nyquist plots of Cu/sCPE (A) and Cu/PAMT/sCPE (B) in 0.5 mol dm^{-3} CH_3OH + 0.5 mol dm^{-3} NaOH. Frequency range: 100 kHz–0.1 Hz; amplitude: 10 mV; bias potential (a → g): 0.3, 0.4, 0.5, 0.6, 0.7, 0.8 and 0.9 V vs SCE. The solid curves are the simulated plots obtained using the equivalent circuit shown in the inset, in which the Warburg impedance was considered only in simulating the plots (e), (f) and (g). The electrodes were prepared under the same conditions as in Fig. 1.

The impedances were fitted using an equivalent circuit in the inset of Fig. 5, where R_s is the solution resistance, Z_w is the Warburg impedance, CPE is the constant phase element, and R_{ct} is the charge-transfer resistance. Z_w was considered only in simulating plots e–g. The CPE is used instead of a capacitor to account for the inhomogeneity of the electrode surface. The fitting curves (solid) were overlaid in Fig. 5, which shows good agreement with the measured data points.

The fitted parameters of the equivalent circuit elements are listed in Table 2, in which Y_0 is the CPE parameter, n is the CPE exponent, and C_{dl} is the double layer capacitance that was calculated according to Eq. (1) proposed by Brug et al. [42],

$$Y_0 = C_{dl}^{n}\left(R_s^{-1} + R_{ct}^{-1}\right)^{1-n} \quad (1)$$

As seen in Table 2, the charge transfer resistance R_{ct} at both electrodes considerably decreased with increasing potential up to 0.6 V, and then tended to stabilize. The R_{ct} values in the higher potential range (0.6–0.9 V) were less than 1.0 Ω cm^2, indicating a very fast electron transfer process at both electrodes. At the potentials lower than 0.6 V, the R_{ct} values of Cu/PAMT/sCPE were markedly smaller than those of Cu/sCPE, which proves that the PAMT interlayer on the sCPE substrate can significantly accelerate the charge transfer kinetics of methanol oxidation in the lower potential range. Meanwhile, both electrodes showed a very large C_{dl} with values of 2.5–10 mF cm^{-2}, reflecting a large specific surface area. At all tested potentials, Cu/PAMT/sCPE had a larger C_{dl} and therefore a larger specific surface area than Cu/sCPE. In addition, the largest Z_w values of both electrodes were observed at 0.7 V, corresponding to the smallest R_{ct} values at the same potential.

3.4. Chronoamperometry

Chronopotentiometric transients were recorded at 0.7 V vs SCE for a long time of 12.2 h, as a measure of the long-term stability of Cu/PAMT/sCPE and Cu/sCPE (Fig. 6, curves a and b). The current densities increased slightly at the first stage, lasting for 18 min for Cu/PAMT/sCPE and 6 min for Cu/sCPE. Then the current densities decreased slowly; the Cu/PAMT/sCPE possessed 67.4% current retention after 12.2 h of continuous operation, which was higher than that of Cu/sCPE (53.3%). By comparison, the presence of PAMT can considerably improve the catalytic efficiency of the laminated Cu particles on methanol oxidation and the stability of the catalysts.

Generally, the chronopotentiometric currents of methanol oxidation at Pt-based electrodes decay rapidly with time due to CO-induced poisoning. The laminated Cu particle electrodes are much more stable than the Pt-based electrodes [3,13], which may be due to the powerful CO-scavenging capability of the laminated Cu particles. This deduction is also supported by the absence of low-frequency inductive loop in EIS. An adsorbed OH radical modulated electron transfer mechanism for the catalytic oxidation of methanol at the surface of the laminated Cu particles is proposed as follows, which is different from the Cu(III)-modulated mechanism.

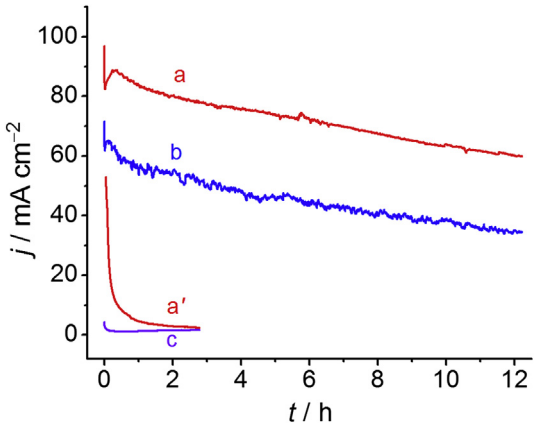

Fig. 6. Chronoamperograms recorded at 0.7 V (vs SCE) on Cu/PAMT/sCPE (a, a′), Cu/sCPE (b) and PAMT/sCPE (c) in 0.5 mol dm^{-3} NaOH in the presence (a, b and c) and absence (a′) of 0.5 mol dm^{-3} CH_3OH. The current densities of curves a′ and c have been magnified by 10 times for clearer view. The electrodes were prepared under the same conditions as in Fig. 1.

$$CuO + OH^- \rightarrow CuO(OH)_{ad} + e^- \quad (2)$$

$$CuO(OH)_{ad} + CH_3OH \rightarrow CuO + CH_3O_{ad} + H_2O \quad (3)$$

$$CuO(OH)_{ad} + CH_3O_{ad} \rightarrow CuO + CH_2O_{ad} + H_2O \quad (4)$$

$$CuO(OH)_{ad} + CH_2O_{ad} \rightarrow CuO + CHO_{ad} + H_2O \quad (5)$$

$$CuO(OH)_{ad} + CHO_{ad} \rightarrow CuO + CO_{ad} + H_2O \quad (6)$$

$$CuO(OH)_{ad} + CO_{ad} + 3OH^- \rightarrow CuO + CO_3^{2-} + 2H_2O + e^- \quad (7)$$

The total reaction may be represented as:

$$CH_3OH + 8OH^- \rightarrow CO_3^{2-} + 6H_2O + 6e^- \quad (8)$$

Table 2
Model parameters simulated from the experimental EIS data in Fig. 5. The equivalent circuit model is shown in the inset of Fig. 5.

Electrode	E/V vs SCE	R_s/ (Ω cm^2)	R_{ct}/ (Ω cm^2)	n	Y_0/(mS s^n cm^{-2})	C_{dl}/mF cm^{-2}	Z_w/ (Ω cm^2)
Cu/sCPE	0.3	1.17	543	0.91	4.22	2.50	
	0.4	1.13	44.1	0.90	8.48	5.05	
	0.5	0.974	2.36	0.87	11.5	5.58	
	0.6	1.04	0.963	0.85	15.1	6.38	
	0.7	1.10	0.704	0.83	15.0	5.34	3.30
	0.8	1.13	0.812	0.82	11.8	3.78	0.323
	0.9	1.30	0.812	0.89	6.72	3.32	0.220
Cu/PAMT/sCPE	0.3	1.48	177	0.89	6.07	3.39	
	0.4	1.24	27.8	0.87	13.3	7.16	
	0.5	1.14	1.80	0.86	18.1	8.88	
	0.6	1.22	0.821	0.85	22.6	10.2	
	0.7	1.29	0.719	0.81	24.8	8.69	4.33
	0.8	1.38	0.922	0.73	33.9	7.79	0.598
	0.9	1.33	0.830	0.87	10.2	4.65	0.274

4. Conclusions

In the present study, we fabricate multi-laminated copper particles on two conductive substrates, using potential-mediated electrochemical deposition. The copper crystallites are preferentially oriented with {111} planes parallel to the substrate surfaces, providing an optimum interface for methanol oxidation. Around individual particles there are a large number of edges, corners, and atomic steps. All these features contribute to the excellent electrocatalytic activity to methanol oxidation. The presence of the conductive polymer PAMT between the carbon paste substrate and the Cu particles results in larger specific surface areas of the particles and smaller charge-transfer resistances of methanol oxidation reaction in the lower potential range. Further development of various preferred oriented non-noble metal materials will enable us to explore novel shape- and orientation-dependent properties for energy, catalysis, sensors, and optoelectronics applications.

Acknowledgment

The authors gratefully acknowledge the financial support from the Specialized Research Fund for the Doctoral Program of Higher Education of China (No. 20130111110025) and the National Nature Science Foundation of China (No. 51203040).

References

[1] S.K. Kamarudin, A.M. Zainoodin, W.R.W. Daud, Int. J. Hydrogen Energy 35 (2010) 4606–4621.
[2] T. Maiyalagan, J. Power Sources 179 (2008) 443–450.
[3] H. Gao, J.-B. He, Y. Wang, N. Deng, J. Power Sources 205 (2012) 164–172.
[4] N. Nakagawa, Y. Ito, T. Tsujiguchi, H. Ishitobi, J. Power Sources 248 (2014) 330–336.
[5] S. Woo, J. Lee, S.-K. Park, H. Kim, T.D. Chung, Y. Piao, J. Power Sources 222 (2013) 261–266.
[6] X. Yu, D. Wang, Q. Peng, Y. Li, Chem. Commun. 47 (2011) 8094–8096.
[7] S. Chereyko, N. Kulyk, C.H. Chung, Langmuir 28 (2012) 3306–3315.
[8] R. Awasthi, R.N. Singh, Carbon 51 (2013) 282–289.
[9] M.-W. Hsieh, T.-J. Whang, Appl. Surf. Sci. 270 (2013) 252–259.
[10] J. Yi, H. Kim, P. Kim, J.B. Joo, W. Kim, I.K. Song, J. Power Sources 157 (2006) 196–200.
[11] R.S. Amin, R.M. Abdel Hameed, K.M. El-Khatib, H. El-Abd, E.R. Souaya, Int. J. Hydrogen Energy 37 (2012) 18870–18881.
[12] O. Guillen-Villafuerte, G. Garcia, R. Guil-Lopez, E. Nieto, J.L. Rodriguez, J.L.G. Fierro, E. Pastor, J. Power Sources 231 (2013) 163–172.
[13] T. Maiyalagan, B. Viswanathan, J. Power Sources 175 (2008) 789–793.
[14] J. Ju, X. Chen, Y. Shi, D. Wu, Fuel 108 (2013) 850–854.
[15] M. Noroozifar, M. Khorasani-Motlagh, M.-S. Ekrami-Kakhki, R. Khaleghian-Moghadam, J. Power Sources 248 (2014) 130–139.
[16] C.S. Sharma, R. Awasthi, R.N. Singh, A.S.K. Sinha, Phys. Chem. Chem. Phys. 15 (2013) 20333–20344.
[17] J.B. Raoof, M.A. Karimi, S.R. Hosseini, S. Mangelizadeh, J. Electroanal. Chem. 638 (2010) 33–38.
[18] S.N. Azizi, S. Ghasemi, E. Chiani, Electrochim. Acta 88 (2013) 463–472.
[19] R. Ojani, J.B. Raoof, S. Fathi, S. Alami-Valikchali, J. Solid State Electrochem. 15 (2011) 1935–1941.
[20] R. Ojani, J.B. Raoof, S.R.H. Zavvarmahalleh, Electrochim. Acta 53 (2008) 2402–2407.
[21] K.L. Nagashree, M.F. Ahmed, J. Solid State Electrochem. 14 (2010) 2307–2320.
[22] L. Zheng, J.F. Song, J. Solid State Electrochem. 14 (2010) 43–50.
[23] J.B. Raoof, R. Ojani, S.R. Hosseini, J. Power Sources 196 (2011) 1855–1863.
[24] R. Ojani, J.-B. Raoof, S. Fathi, J. Solid State Electrochem. 13 (2009) 927–934.
[25] R. Ojani, J.B. Raoof, S. Fathi, Electrochim. Acta 54 (2009) 2190–2196.
[26] H. Heli, M. Jafarian, M.G. Mahjani, F. Gobal, Electrochim. Acta 49 (2004) 4999–5006.
[27] S. Carugno, E. Chassaing, M. Rosso, G.A. González, Mater. Chem. Phys. 143 (2014) 1012–1017.
[28] R. Venkatasubramanian, J. He, M.W. Johnson, I. Stern, D.H. Kim, N.S. Pesika, Langmuir 29 (2013) 13135–13139.
[29] A.P. Periasamy, J. Liu, H.-M. Lin, H.-T. Chang, J. Mater. Chem. A 1 (2013) 5973–5981.
[30] R. Ojani, J.-B. Raoof, Y. Ahmady-Khanghah, Electrochim. Acta 56 (2011) 3380–3386.
[31] J. Li, L. Li, Y. Yu, Y. Gao, J. Liu, J. Rare Earths 31 (2013) 296–301.
[32] N.A.M. Barakat, M. El-Newehy, S.S. Al-Deyab, H.Y. Kim, Nanoscale Res. Lett. 9 (2014) 2.
[33] R.M.A. Hameed, K.M. El-Khatib, Int. J. Hydrogen Energy 35 (2010) 2517–2529.
[34] M.U.A. Prathap, R. Srivastava, Nano Energy 2 (2013) 1046–1053.
[35] X. Niu, Y. Li, J. Tang, Y. Hu, H. Zhao, M. Lan, Biosens. Bioelectron. 51 (2014) 22–28.
[36] J.-B. He, F. Qi, Y. Wang, N. Deng, Sens. Actuators B 145 (2010) 480–487.
[37] J.-B. He, D.-Y. Lu, G.-P. Jin, Appl. Surf. Sci. 253 (2006) 689–697.
[38] Y.-H. Wang, J.-B. He, Electrochim. Acta 66 (2012) 45–51.
[39] Y. Xie, C.O. Huber, Anal. Chem. 63 (1991) 1714–1719.
[40] J.T. Müller, P.M. Urban, W.F. Hölderich, J. Power Sources 84 (1999) 157–160.
[41] D.A. Harrington, B.E. Conway, Electrochim. Acta 32 (1987) 1703–1712.
[42] G.J. Brug, A.L.G. Vandeneeden, M. Sluytersrehbach, J.H. Sluyters, J. Electroanal. Chem. Interfacial Electrochem. 176 (1984) 275–295.